Research Article

Humaira Yasmin*, Ali M. Mahnashi, Waleed Hamali, Showkat Ahmad Lone, and Anwar Saeed*

HAM simulation for bioconvective magnetohydrodynamic flow of Walters-B fluid containing nanoparticles and microorganisms past a stretching sheet with velocity slip and convective conditions

https://doi.org/10.1515/phys-2023-0140
received September 16, 2023; accepted October 30, 2023

Abstract: In recent years, many numerical and analytical attempts have been reported by the researchers to explore the technological and industrial processes. Thermal management, hybrid-powered engine, microelectronics, heat exchanger, solar systems, energy generators are some recent applications of the heat and mass transfer flow. In this article, we have theoretically analyzed the convection flow of Walters-B fluid past a vertical extending surface. The Walters-B nanofluid contains the gyrotactic microorganisms and nanoparticles. The slip and convective conditions are imposed on the velocity and temperature equations. The modeled equations are reformed into the system of ordinary differential equations. Further, the transformed ordinary differential equations are solved analytically. The analytical results are compared with numerical solution and have found great resemblance to each other. The convergence analysis of analytical solution is also presented in this study. The impacts of the embedded factors on Walters-B nanofluid have been presented and deliberated in detail. The results show that the improvement in viscoelastic and magnetic parameter declined the nanofluid motion for both slip and no-slip conditions. The escalated mixed convection parameter has augmented the nanofluid motion. Additionally, at the surface of sheet, the slip condition reduces the fluid motion, however, away from the stretching surface, an increasing conduct up-to some points and then free stream velocity is found. The increased bioconvection Lewis number has increased the microorganisms' profile while the greater bioconvection Peclet number has increased the microorganisms' profiles reduced. The streamline patterns for Newtonian, non-Newtonian, magnetized, and non-magnetized cases have different behaviors. The flow factors have dominant impact on velocity profiles for the case of slip condition.

Keywords: Walters-B nanofluid, gyrotactic microorganisms, nanoparticles, MHD, mixed convection, bioconvection, binary chemical reaction, Arrhenius activation energy, analytical and numerical approaches

*** Corresponding author: Humaira Yasmin,** Department of Basic Sciences, General Administration of the Preparatory Year, King Faisal University, 31982, Al Ahsa, Saudi Arabia, e-mail: hhassain@kfu.edu.sa
*** Corresponding author: Anwar Saeed,** Department of Mathematics, Abdul Wali Khan University, Mardan, 23200, Khyber Pakhtunkhwa, Pakistan, e-mail: anwarsaeed769@gmail.com
Ali M. Mahnashi, Waleed Hamali: Department of Mathematics, College of Science, Jazan University, Jazan, Saudi Arabia
Showkat Ahmad Lone: Department of Basic Sciences, College of Science and Theoretical Studies, Saudi Electronic University, Jeddah-M, Riyadh 11673, Saudi Arabia

Nomencalture

$\widehat{a_1}$, $\widehat{a_2}$, $\widehat{a_3}$, Δ_1	constants
B	magnetic field
$\widehat{C}$	nanoparticles' concentrations
E	activation energy
$\widehat{g}$	gravitational force
Le	bioconvection Lewis number
M	magnetic field parameter
$\widehat{N}$	microorganisms' concentrations
Nb	Brownian motion
Nc	Rayleigh number
Nr	buoyancy ratio term
Nt	thermophoresis term
Nu_x	Nusselt number
Pe	Peclet number
Pr	Prandtl number
Rd	thermal radiation

Sh_x	Sherwood number
$\widehat{u_w} = \widehat{a}\,\widehat{x}$	stretching velocity
α	slip parameter
β	viscoelastic parameter
ω	chemical reaction parameter
$\widehat{T}$	temperature
λ_C	concentration relaxation factor
λ_E	thermal relaxation factor
γ_1	thermal Biot number
γ_2	nanoparticles Biot number
γ_3	microorganisms Biot number
λ	mixed convection factor
σ	temperature difference

1 Introduction

The nonlinear connection between shear stress and deformation rate at a given pressure and temperature characterizes non-Newtonian fluids (NNFs). Such fluid flows are widespread in a variety of industrial applications, including thermal oil recovery, discharge of industrial pollutants, food, polymer processing, *etc*. Non-Newtonian boundary layer flows have numerous industrial uses, including fabrication, cooling of metallic plates, layering onto rigid substrates, aerodynamic extrusion of plastic sheets, and coating application. Many studies have increasingly looked into such flows, taking into account a variety of factors. Turkyilmazoglu [1] investigated the viscoelastic flow of electrically conducting fluid through an extending/shrinking surface using porous media. Hosseini *et al.* [2] reported the thermal and mass transmissions across NNFs flow. They found that the increasing Reynolds number augments the heat transfer rate. Abbasbandy *et al.* [3] documented the magnetohydrodynamic (MHD) flow of Maxwell fluid flow. Their consequences disclosed that augmenting magnetic parameter has declined the velocity profile. Yang and Zhu [4] scrutinized the fluid flow in an infinite long straight pipe. They concluded that oscillations happen just before fluid reaches the abovementioned asymptotic behavior, which is really a regular phenomenon in viscoelastic fluids. Hayat *et al.* [5] investigated the chemically reactive viscoelastic fluid flow past an extending surface with Dufour and Soret influences. Their results showed that the Dufour and Soret numbers have opposite effects on the flow behavior. Hayat *et al.* [6] considered the MHD micropolar fluid flow past an extending surface with mixed convection phenomenon. Their result disclosed that the strong concentration has a parabolic impact on microrotation field. Jamil *et al.* [7] presented the comparative valuation of NNFs flow between two coaxial circular cylinders. They found that the velocity of the Newtonian fluid is faster than the NNFs. Mustafa *et al.* [8] offered the comparative flow of viscous and Casson fluids at stagnation point past an extending surface. It has been concluded that the magnitudes of surface drag force and velocity are dominant for the case of Casson fluid than viscous fluid. Mushtaq *et al.* [9] examined the Maxwell fluid flow with thermal radiation influence. It has been introduced that the thermal radiation has augmented the temperature of the Maxwell fluid flow. Hayat *et al.* [10] scrutinized the NNFs flow across and extending sheet. Their results showed that the energy curve of the third-grade fluid flow augment with the augmenting electric field.

Viscoelastic fluids are a type of NNFs. These fluids have both viscous and elastic properties. In the paper and petroleum industries, geophysical fluid dynamics, and chemical technologies, viscoelastic flow is becoming increasingly important. Thus, Bhatia and Steiner [11] looked into the instability of heat in a viscoelastic fluid when it rotates. They found that the destabilizing impact of fluid flow. Though, their model does not deliberate all the features of a viscoelastic fluid. Walters-B fluid model is the best model for describing such fluid because of its relevance. Beard and Walters [12] presented the viscoelastic liquid at a stagnation point. Sharma and Gupta [13] analyzed the MHD viscoelastic Walters-B fluid through a stratified medium. Nandeppanavar *et al.* [14] analyzed the thermal transmission characteristics of the Walters-B fluid past an extending sheet. Abdul Hakeem *et al.* [15] presented the thermal transmission examination of Walters-B fluid flow across an extending surface. They concluded that the fluid temperature decreases for the combined effects of thermal radiation with elastic deformation, viscoelastic field, Prandtl number, and Eckert number. Makinde *et al.* [16] examined the electrically conducting Walters-B fluid with velocity slip condition. Tahir *et al.* [17] determined the exact solutions for the rotating flow of Oldroyd-B, fractional Newtonian, and Maxwell fluids through an annulus. Waqas *et al.* [18] addressed the Darcy–Forchheimer fluid flow over an extending plate/cylinder with mass and heat fluxes, motile microbes. It was assumed that fluid velocity falloffs with the influence of mixed convection and local inertia factor. Imran *et al.* [19] studied the impact of thermal radiation and melting phenomena through bioconvective nanofluid flow with movable microbes across a cylinder. It has been shown that enhancing the computed value of a mixed convection improves the velocity. Ibrahim *et al.* [20] discussed the MHD radiative stagnation point flow across a stretching surface taking into account Brownian and thermophoresis effect. Increases in the velocity and magnetic constraints were discovered to dampen fluid velocity, whereas thermophoresis effect emphasizes specific thermal properties. Kumar *et al.* [21] used the homotopy

analysis method (HAM) approach to investigate the effect of slip function on MHD flow of Casson nanoliquid across a porous extending surface. It was discovered that increasing the velocity slip factor causes an increase in fluid velocity, whereas increasing the thermal slip factor causes a decrease in the distribution of heat. Sekhar *et al.* [22] and Harish *et al.* [23] reviewed the effect of MHD Casson nanoliquid flow through a tilted extending sheet with heat source/sink, thermal radiation, and Soret and Dufour effect. Swain *et al.* [24] used the numerical perspective bvp4c package to investigate the impact of Joule heating and exponential heat source on the nanofluid flow. Some recent reports on Walters-B fluid are cited in the literature [25–34].

Farooq *et al.* [35,36] studied the three-dimensional flow of a hybrid nanofluid composed of Nichrome 80% Ni, 20% Cr, and TC4 (Ti–6A–14V) nanoparticles combined within engine oil to improve the mass and heat exchange rate. Wakif *et al.* [37] conducted a systematic review on the consequences of tiny particles that are subjected to thermophoretic effect and realized that the effect of thermal radiation has a significant impact on the relevance of tiny particle migration through the fluid flow. Manigandan and Satya Narayana [38] and Madiha Takreem and Satya Narayana [39] numerically investigated the mixed convection steady (SWCNT + MWCNT/H_2O) hybrid nanoliquid flow with the effect of variable thermal conductivity, slip boundary conditions, thermal radiation, and heat generation through prolonging surface. The results of the thermal slip evaluation towards an elastic sheet demonstrate that the hybrid nanoliquid advances the efficiency of heat dissemination by 4.33%. Harish Babu *et al.* [40,41] assessed the effects of thermal heat flux, velocity slip, and an inclined magnetic field on the hybrid nanofluids flow across an exponentially extended sheet. Venkateswarlu and Satya Narayana [42] assessed the impact of radiating Coriolis force and wall velocity on the convective flow across an impermeable vertical sheets in a spinning fluid induced by a viscous dissipation and magnetic field. Zhang *et al.* [43] evaluated the 2D flow and thermodynamic properties of a radiated consistent hybrid nanoliquid across a fixed wedge, using an application of Falkner–Skan flows. Wakif and Shah [44] quantitatively characterized the various physical highlights of MHD steady flow over a spinning disc. Ragupathi *et al.* [45] reported the heat transfer and bio-convective MHD flow of nanoliquid caused by the floating of gyrotactic organisms across a conical pulled sheet. The dispersion of motile microbes toward the curvature factor was shown to be reducing extensively. Rasool *et al.* [46] and Areekara *et al.* [47] calculated the heterogeneous hybrid nanoliquid flow consisting of water, silver, and molybdenum oxide fine particles on a rigid wedge surface embedded in a Darcy medium. The amplification of radiative heat flux was shown to greatly enhance the surface heat dissipation rate.

Inspired by the above uses, applications, and studies based on different physical phenomena, the aim of the current analysis is to consider the mixed convection flow past a vertical stretching surface. In the present analysis, we have considered the impacts of binary chemical reaction, magnetic field, Brownian motion, and thermal radiation. Additionally, the velocity slip condition, and convective conditions are taken into consideration. The Cattaneo–Christov heat and mass flux model is also considered in the present investigation in order to investigate the heat and mass transfer flow. Section 2 presents the mathematical model for the proposed model. Section 3 shows the semi-analytical solution of the proposed model. The outcomes of the present analysis and their physical discussion are presented in Section 4. The final outcomes of the present analysis are listed in Section 5.

2 Problem formulation

Assume the steady and laminar flow of Walters-B fluid past an elongating sheet. The stretching velocity $\widehat{u}_w = \widehat{a}\,\widehat{x}$ is taken along $\widehat{x}$-direction. The gravitational force represented by $\widehat{g}$, is performed in downward direction as shown in Figure 1. The temperature of the sheet is represented by $\widehat{T}$. Furthermore, the nanoparticles and gyrotactic microorganisms' concentrations are denoted by $\widehat{C}$ and $\widehat{N}$. In $\widehat{y}$-direction the magnetic field of strength B_0 is applied. The convective and slip conditions are also considered.

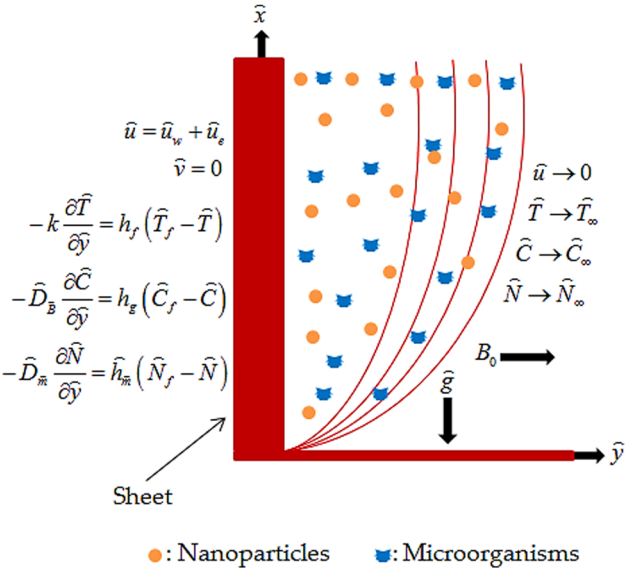

Figure 1: Geometrical representation of the flow problem.

The Cattaneo–Christov heat and mass flux model is also considered in the present investigation in order to investigate the heat and mass transfer flow. Based on the above assumptions, the problem is formulated as [25–28] follows:

$$\frac{\partial \widehat{u}}{\partial \widehat{x}} + \frac{\partial \widehat{v}}{\partial \widehat{y}} = 0, \tag{1}$$

$$\begin{aligned}
&\widehat{u}\frac{\partial \widehat{u}}{\partial \widehat{x}} + \widehat{v}\frac{\partial \widehat{u}}{\partial \widehat{y}} \\
&= \frac{\widehat{\mu}}{\widehat{\rho}}\frac{\partial^2 \widehat{u}}{\partial \widehat{y}^2} - \frac{k_0}{\widehat{\rho}} \\
&\left[\widehat{u}\frac{\partial^3 \widehat{u}}{\partial \widehat{x}\,\partial \widehat{y}^2} + \widehat{v}\frac{\partial^3 \widehat{u}}{\partial \widehat{y}^3} + \frac{\partial^2 \widehat{u}}{\partial \widehat{y}^2}\frac{\partial \widehat{u}}{\partial \widehat{x}} - \frac{\partial^2 \widehat{u}}{\partial \widehat{x}\,\partial \widehat{y}}\frac{\partial \widehat{u}}{\partial \widehat{y}}\right], \\
&- \frac{\widehat{\sigma} B_0^2}{\widehat{\rho}}\widehat{u} + \frac{1}{\widehat{\rho}}\left[\begin{array}{l}(\widehat{\rho}\,\widehat{\beta})\widehat{g}(\widehat{T} - \widehat{T}_\infty) - \\ \left(\frac{\widehat{M}_{\mathrm{p}}(\widehat{\rho}_{\mathrm{p}} - \widehat{\rho}_{\mathrm{f}})\widehat{g}}{\widehat{\rho}_{\mathrm{p}}}\right)(\widehat{C} - \widehat{C}_\infty) - \\ \widehat{\gamma}(\widehat{\rho}_{\mathrm{m}} - \widehat{\rho}_{\mathrm{f}})\widehat{g}(\widehat{N} - \widehat{N}_\infty)\end{array}\right]
\end{aligned} \tag{2}$$

$$\begin{aligned}
&\widehat{u}\frac{\partial \widehat{T}}{\partial \widehat{x}} + \widehat{v}\frac{\partial \widehat{T}}{\partial \widehat{y}} \\
&= \left(\frac{\widehat{k}}{(\widehat{\rho}\,\widehat{C}_{\mathrm{p}})} + \frac{16\sigma^* \widehat{T}_\infty^3}{3k^*}\right)\frac{\partial^2 \widehat{T}}{\partial \widehat{y}^2} \\
&+ \tau\left(\frac{\widehat{D}_{\widehat{B}}\widehat{M}_{\mathrm{p}}}{\widehat{\rho}_{\mathrm{p}}}\frac{\partial \widehat{C}}{\partial \widehat{y}} + \frac{\widehat{D}_{\widehat{T}}}{\widehat{T}_\infty}\frac{\partial \widehat{T}}{\partial \widehat{y}}\right) - \delta_{\mathrm{E}} \\
&\left(\begin{array}{l}\widehat{u}\frac{\partial \widehat{T}}{\partial \widehat{x}}\frac{\partial \widehat{u}}{\partial \widehat{x}} + \widehat{v}\frac{\partial \widehat{T}}{\partial \widehat{y}}\frac{\partial \widehat{v}}{\partial \widehat{y}} + \widehat{u}^2\frac{\partial^2 \widehat{T}}{\partial \widehat{x}^2} \\ + \widehat{v}^2\frac{\partial^2 \widehat{T}}{\partial \widehat{y}^2} + \\ 2\widehat{u}\,\widehat{v}\frac{\partial^2 \widehat{T}}{\partial \widehat{x}\,\partial \widehat{y}} + \widehat{u}\frac{\partial \widehat{T}}{\partial \widehat{y}}\frac{\partial \widehat{v}}{\partial \widehat{x}} + \widehat{v}\frac{\partial \widehat{T}}{\partial \widehat{x}}\frac{\partial \widehat{u}}{\partial \widehat{y}}\end{array}\right),
\end{aligned} \tag{3}$$

$$\begin{aligned}
&\widehat{u}\frac{\partial \widehat{C}}{\partial \widehat{x}} + \widehat{v}\frac{\partial \widehat{C}}{\partial \widehat{y}} \\
&= \widehat{D}_{\widehat{B}}\left(\frac{\partial^2 \widehat{C}}{\partial \widehat{y}^2}\right) + \frac{\widehat{D}_{\widehat{T}}}{\widehat{T}_\infty}\frac{\widehat{\rho}_{\mathrm{p}}}{\widehat{M}_{\mathrm{p}}}\frac{\partial^2 \widehat{T}}{\partial \widehat{y}^2} \\
&- \widehat{k}_{\mathrm{r}}^2(\widehat{C} - \widehat{C}_\infty)\left(\frac{\widehat{T}}{\widehat{T}_\infty}\right)^n \exp\left[-\frac{\widehat{E}_{\widehat{a}}}{\widehat{k}_{\widehat{B}}\widehat{T}}\right] \\
&- \delta_{\widehat{C}}\left(\begin{array}{l}\widehat{u}\frac{\partial \widehat{C}}{\partial \widehat{x}}\frac{\partial \widehat{u}}{\partial \widehat{x}} + \widehat{v}\frac{\partial \widehat{C}}{\partial \widehat{y}}\frac{\partial \widehat{v}}{\partial \widehat{y}} + \widehat{u}^2\frac{\partial^2 \widehat{C}}{\partial \widehat{x}^2} + \\ \widehat{v}^2\frac{\partial^2 \widehat{C}}{\partial \widehat{y}^2} + 2\widehat{u}\,\widehat{v}\frac{\partial^2 \widehat{C}}{\partial \widehat{x}\,\partial \widehat{y}} + \widehat{u}\frac{\partial \widehat{C}}{\partial \widehat{y}}\frac{\partial \widehat{v}}{\partial \widehat{x}}, \\ + \widehat{v}\frac{\partial \widehat{C}}{\partial \widehat{x}}\frac{\partial \widehat{u}}{\partial \widehat{y}}\end{array}\right)
\end{aligned} \tag{4}$$

$$\begin{aligned}
&\widehat{u}\frac{\partial \widehat{N}}{\partial \widehat{x}} + \widehat{v}\frac{\partial \widehat{N}}{\partial \widehat{y}} + \frac{\widehat{b}_{\mathrm{c}}\widehat{W}_{\mathrm{c}}}{(\widehat{C}_{\mathrm{f}} - \widehat{C}_\infty)}\frac{\partial \widehat{N}}{\partial \widehat{y}}\frac{\partial \widehat{C}}{\partial \widehat{y}} + \frac{\widehat{b}_{\mathrm{c}}\widehat{W}_{\mathrm{c}}}{(\widehat{C}_{\mathrm{f}} - \widehat{C}_\infty)} \\
&\widehat{N}\frac{\partial^2 \widehat{C}}{\partial \widehat{y}^2} = \widehat{D}_{\widehat{m}}\frac{\partial^2 \widehat{N}}{\partial \widehat{y}^2},
\end{aligned} \tag{5}$$

with boundary conditions [48,49]

$$\left\{\begin{array}{l}\widehat{u} = \widehat{u}_{\mathrm{w}} + \widehat{u}_{\mathrm{slip}},\ -\frac{\partial \widehat{T}}{\partial \widehat{y}} = \frac{h_{\mathrm{f}}}{k}(\widehat{T}_{\mathrm{f}} - \widehat{T}),\ \widehat{v} = 0, \\ -\frac{\partial \widehat{C}}{\partial \widehat{y}} = \frac{h_g}{\widehat{D}_{\widehat{B}}}(\widehat{C}_{\mathrm{f}} - \widehat{C}),\ -\frac{\partial \widehat{N}}{\partial \widehat{y}} = \frac{\widehat{h}_{\widehat{m}}}{\widehat{D}_{\widehat{m}}}(\widehat{N}_{\mathrm{f}} - \widehat{N}) \\ \text{at}\ \widehat{y} = 0, \\ \quad \widehat{u} \to 0,\ \widehat{C} \to \widehat{C}_\infty,\ \widehat{T} \to \widehat{T}_\infty, \\ \quad \widehat{N} \to \widehat{N}_\infty\ \text{as}\ \widehat{y} \to \infty.\end{array}\right\} \tag{6}$$

where

$$\left\{\begin{array}{l}\widehat{u}_{\mathrm{w}} = \widehat{a}\,\widehat{x},\ \widehat{u}_{\mathrm{slip}} = \Delta_1\frac{\partial \widehat{u}}{\partial \widehat{y}},\ \widehat{C}_{\mathrm{f}} = \widehat{C}_\infty + \widehat{x}\,\widehat{a}_2,\ \widehat{T}_{\mathrm{f}} = \\ \widehat{T}_\infty + \widehat{a}_1\widehat{x},\ \widehat{N}_{\mathrm{f}} = \widehat{N}_\infty + \widehat{a}_3\widehat{x}.\end{array}\right\} \tag{7}$$

in which $\widehat{a}_1$, $\widehat{a}_2$, $\widehat{a}_3$, and Δ_1 are constants.

The similarity transformations are defined as [49] follows:

$$\begin{aligned}
&\widehat{u} = \widehat{a}\,\widehat{x}f'(\xi),\ \widehat{v} = -\sqrt{\upsilon_{\mathrm{f}}\widehat{a}}\,f(\eta),\ \theta(\xi) = \frac{\widehat{T} - \widehat{T}_\infty}{\widehat{T}_{\mathrm{f}} - \widehat{T}_\infty}, \\
&\chi(\xi) = \frac{\widehat{N} - \widehat{N}_\infty}{\widehat{N}_{\mathrm{f}} - \widehat{N}_\infty},\ \phi(\xi) = \frac{\widehat{C} - \widehat{C}_\infty}{\widehat{C}_{\mathrm{f}} - \widehat{C}_\infty},\ \xi = \sqrt{\frac{\widehat{a}}{\upsilon_{\mathrm{f}}}}\widehat{y}.
\end{aligned} \tag{8}$$

Using the above similarity transformations, we obtain

$$\begin{aligned}
&\frac{\partial^3 f}{\partial \xi^3} - \left(\frac{\partial f}{\partial \xi}\right)^2 + f\frac{\partial^2 f}{\partial \xi^2} - M\frac{\partial f}{\partial \xi} \\
&- \beta\left(2\frac{\partial f}{\partial \xi}\frac{\partial^3 f}{\partial \xi^3} - f\frac{\partial^4 f}{\partial \xi^4} - \left(\frac{\partial^2 f}{\partial \xi^2}\right)^2\right) \\
&+ \lambda(\theta - \mathrm{Nr}\phi - \mathrm{Nc}\chi) = 0,
\end{aligned} \tag{9}$$

$$\begin{aligned}
&\frac{(1 + \mathrm{Rd})}{\mathrm{Pr}}\frac{\partial^2 \theta}{\partial \xi^2} - \theta\frac{\partial f}{\partial \xi} + f\frac{\partial \theta}{\partial \xi} + \mathrm{Nb}\frac{\partial \theta}{\partial \xi}\frac{\partial \phi}{\partial \xi} \\
&+ \mathrm{Nt}\left(\frac{\partial \theta}{\partial \xi}\right)^2 - \lambda_{\mathrm{E}} \\
&\left(\theta\left(\frac{\partial f}{\partial \xi}\right)^2 - f\theta\frac{\partial^2 f}{\partial \xi^2} - f\frac{\partial \theta}{\partial \xi}\frac{\partial f}{\partial \xi} + f^2\frac{\partial^2 \theta}{\partial \xi^2}\right) = 0,
\end{aligned} \tag{10}$$

$$\frac{\partial^2\phi}{\partial\xi^2} + \frac{\mathrm{Nt}}{\mathrm{Nb}}\frac{\partial^2\theta}{\partial\xi^2} - \mathrm{PrLe}\lambda_{\mathrm{C}}\left(\phi\left(\frac{\partial f}{\partial\xi}\right)^2 - f\phi\frac{\partial^2 f}{\partial\xi^2} - f\frac{\partial f}{\partial\xi}\frac{\partial\phi}{\partial\xi} + f^2\frac{\partial^2\phi}{\partial\xi^2}\right) + \mathrm{LePr}\left(f\frac{\partial\phi}{\partial\xi} - \phi\frac{\partial f}{\partial\xi}\right) - \mathrm{PrLe}\omega\phi(\sigma\theta+1)^n \times \exp\left(-\frac{E}{\sigma\theta+1}\right) = 0, \tag{11}$$

$$\frac{\partial^2\chi}{\partial\xi^2} + \mathrm{LbPr}\left(f\frac{\partial\chi}{\partial\xi} - \chi\frac{\partial f}{\partial\xi}\right) - \mathrm{Pe}\left(\frac{\partial\phi}{\partial\xi}\frac{\partial\chi}{\partial\xi} + \chi\frac{\partial^2\phi}{\partial\xi^2} + \delta\frac{\partial^2\phi}{\partial\xi^2}\right) = 0, \tag{12}$$

with boundary conditions

$$\left.\begin{aligned} &f(0) = 0,\ \frac{\partial f(0)}{\partial\xi} = 1 + \alpha\frac{\partial^2 f(0)}{\partial\xi^2},\ \frac{\partial f(\infty)}{\partial\xi} \to 0,\\ &\frac{\partial\theta(0)}{\partial\xi} = -\gamma_1(1-\theta(0)),\ \theta(\infty)\to 0,\\ &\frac{\partial\phi(0)}{\partial\xi} = -\gamma_2(1-\phi(0)),\ \phi(\infty)\to 0,\\ &\frac{\partial\chi(0)}{\partial\xi} = -\gamma_3(1-\chi(0)),\ \chi(\infty)\to 0. \end{aligned}\right\} \tag{13}$$

The embedded parameters and their default values are defined in Table 1.

The engineering interest quantities are stated as follows:

$$S_{fx} = \frac{2}{\rho u_{\mathrm{w}}^2}\left[\mu\frac{\partial\widehat{u}}{\partial\widehat{y}}\right|_{\widehat{y}=0} - k_0\left(\widehat{u}\frac{\partial^2\widehat{u}}{\partial\widehat{x}\,\partial\widehat{y}} + \widehat{v}\frac{\partial^2\widehat{u}}{\partial\widehat{y}^2} + 2\frac{\partial\widehat{u}}{\partial\widehat{y}}\frac{\partial\widehat{u}}{\partial\widehat{x}}\right)\Bigg|_{\widehat{y}=0}\Bigg], \tag{14}$$

$$\mathrm{Nu}_x = -\frac{\widehat{x}}{\widehat{k}(\widehat{T}_{\mathrm{f}} - \widehat{T}_\infty)}\left(k + \frac{16\sigma^*\widehat{T}_\infty^3}{3k^*}\right)\frac{\partial\widehat{T}}{\partial\widehat{y}}\Bigg|_{\widehat{y}=0}, \tag{15}$$

$$\mathrm{Sh}_x = -\frac{\widehat{x}}{\widehat{k}(\widehat{C}_{\mathrm{f}} - \widehat{C}_\infty)}\frac{\partial\widehat{C}}{\partial\widehat{y}}\Bigg|_{\widehat{y}=0}, \tag{16}$$

$$\mathrm{Nm}_x = -\frac{\widehat{x}}{(\widehat{N}_{\mathrm{f}} - \widehat{N}_\infty)}\frac{\partial\widehat{N}}{\partial\widehat{y}}\Bigg|_{\widehat{y}=0}. \tag{17}$$

Table 1: Embedded parameters and their default values

Parameter	Name	Default value
$M = \frac{\widehat{\sigma}B_0^2}{a\widehat{\rho}}$	Magnetic parameter	1.5
$\gamma_1 = \frac{h_{\mathrm{f}}}{k}\sqrt{\frac{\upsilon_{\mathrm{f}}}{\widehat{a}}}$	Thermal Biot number	0.2
$\gamma_2 = \frac{h_{\mathrm{g}}}{\widehat{D}_{\widehat{B}}}\sqrt{\frac{\upsilon_{\mathrm{f}}}{\widehat{a}}}$	Nanoparticles Biot number	0.2
$\gamma_3 = \frac{\widehat{h}_{\widehat{m}}}{\widehat{D}_{\widehat{m}}}\sqrt{\frac{\upsilon_f}{\widehat{a}}}$	Microorganisms Biot number	0.2
$\lambda = \frac{g\widehat{\beta}(\widehat{T}_{\mathrm{f}} - \widehat{T})}{\widehat{a}\,\widehat{u}_{\mathrm{w}}}$	Mixed convection factor	0.5
$\mathrm{Nc} = \frac{\widehat{\gamma}(\widehat{\rho}_{\mathrm{m}} - \widehat{\rho}_{\mathrm{f}})(\widehat{N}_{\mathrm{f}} - \widehat{N}_\infty)}{(\widehat{\rho}\,\widehat{\beta})(\widehat{T}_{\mathrm{f}} - \widehat{T}_\infty)}$	Rayleigh number	0.8
$\mathrm{Nr} = \frac{\widehat{M}_{\mathrm{p}}(\widehat{\rho}_{\mathrm{p}} - \widehat{\rho}_{\mathrm{f}})(\widehat{C}_{\mathrm{f}} - \widehat{C}_\infty)}{\widehat{\rho}_{\mathrm{p}}(\widehat{\rho}\,\widehat{\beta})(\widehat{T}_{\mathrm{f}} - \widehat{T}_\infty)}$	Buoyancy ratio term	0.4
$\lambda_{\mathrm{C}} = \widehat{a}\,\delta_{\widehat{C}}$	Concentration relaxation factor	0.5
$\lambda_{\mathrm{E}} = \widehat{a}\,\delta_{\widehat{T}}$	Thermal relaxation factor	0.5
$\mathrm{Nt} = \frac{\tau\widehat{D}_{\widehat{T}}(\widehat{T}_{\mathrm{f}} - \widehat{T}_\infty)}{\widehat{T}_\infty\upsilon_{\mathrm{f}}}$	Thermophoresis factor	0.5
$\mathrm{Nb} = \frac{\tau\widehat{M}_{\mathrm{p}}\widehat{D}_{\widehat{B}}(\widehat{C}_{\mathrm{f}} - \widehat{C}_\infty)}{\widehat{\rho}_{\mathrm{p}}\upsilon_{\mathrm{f}}}$	Brownian motion factor	0.5
$\mathrm{Rd} = \frac{16\sigma^*\widehat{T}_\infty^3}{3kk^*}$	Thermal radiation factor	0.2
$\mathrm{Pr} = \frac{(\widehat{\rho}\,\widehat{C}_{\mathrm{p}})\upsilon_{\mathrm{f}}}{\widehat{k}}$	Prandtl number	6.0
$\omega = \frac{\widehat{k}_{\mathrm{r}}^2}{\widehat{a}}$	Chemical reaction parameter	0.1
$\mathrm{Le} = \frac{\widehat{k}}{(\widehat{\rho}\,\widehat{C}_{\mathrm{p}})\widehat{D}_{\widehat{B}}}$	Bioconvection Lewis number	0.2
$\sigma = \frac{(\widehat{T}_{\mathrm{f}} - \widehat{T}_\infty)}{\widehat{T}_\infty}$	Temperature difference parameter	0.6
$E = \frac{\widehat{E}_{\widehat{a}}}{\widehat{k}_{\widehat{B}}\widehat{T}_\infty}$	Activation energy parameter	0.3
$\mathrm{Pe} = \frac{\widehat{b}_{\mathrm{c}}\widehat{W}_{\mathrm{c}}}{\widehat{D}_{\widehat{m}}}$	Bioconvection Peclet number	0.2
$\alpha = \Delta_1\sqrt{\frac{\widehat{a}}{\upsilon_{\mathrm{f}}}}$	Slip parameter	0.2
$\beta = \frac{k_0\widehat{a}}{\widehat{\mu}}$	Viscoelastic parameter	0.4

Using Eq. (8), Eqs. (14)–(17) are reduced as follows:

$$\sqrt{\mathrm{Re}_x}\,C_{fx} = 2(1-3\beta)\frac{\partial^2 f(0)}{\partial\xi^2}. \tag{18}$$

$$\frac{\mathrm{Nu}_x}{\sqrt{\mathrm{Re}_x}} = -(1+\mathrm{Rd})\frac{\partial\theta(0)}{\partial\xi}. \tag{19}$$

$$\frac{\mathrm{Sh}_x}{\sqrt{\mathrm{Re}_x}} = -\frac{\partial\phi(0)}{\partial\xi}. \tag{20}$$

$$\frac{\mathrm{Nm}_x}{\sqrt{\mathrm{Re}_x}} = -\frac{\partial\chi(0)}{\partial\xi}. \tag{21}$$

3 HAM solution

First presented by Liao [50], the HAM is a general approximate analytical technique for solving series of nonlinear problems of different kinds, such as ordinary differential equations, differential–integral equations, coupled equations, differential–difference equations, algebraic equations, and partial differential equations. This approach is applicable to any nonlinear problems, regardless of how many physical factors are involved, which is basically necessary for perturbation approaches. More crucially, the HAM gives us a choice to select appropriate base functions for approximation of a nonlinear problem and a straightforward method to guarantee the convergence of the solution series, unlike all perturbation and conventional non-perturbation methods. To solve the proposed model, the initial guesses are taken as follows:

$$\left.\begin{aligned} f_0(\xi) &= \frac{1}{1+\alpha}(1-e^{(-\xi)}),\ \theta_0(\xi) = \frac{\gamma_1}{1+\gamma_1}(e^{(-\xi)}),\\ \phi_0(\xi) &= \frac{\gamma_2}{1+\gamma_2}(e^{(-\xi)}),\ \chi_0(\xi) = \frac{\gamma_3}{1+\gamma_3}(e^{(-\xi)}). \end{aligned}\right\} \tag{22}$$

$$\left.\begin{aligned} L_f[f(\xi)] &= f''' - f',\\ L_\theta[\theta(\xi)] &= \theta'' - \theta,\\ L_\phi[\phi(\xi)] &= \phi'' - \phi,\\ L_\chi[\chi(\xi)] &= \chi'' - \chi. \end{aligned}\right\} \tag{23}$$

with

$$\left.\begin{aligned} L_f[\mathbb{N}_1 + \mathbb{N}_2 e^{(-\xi)} + \mathbb{N}_3 e^{(\xi)}] &= 0,\\ L_\theta[\mathbb{N}_4 e^{(-\xi)} + \mathbb{N}_5 e^{(\xi)}] &= 0,\\ L_\phi[\mathbb{N}_6 e^{(-\xi)} + \mathbb{N}_7 e^{(\xi)}] &= 0,\\ L_\chi[\mathbb{N}_8 e^{(-\xi)} + \mathbb{N}_9 e^{(\xi)}] &= 0. \end{aligned}\right\} \tag{24}$$

where $\mathbb{N}_1, \mathbb{N}_2, \mathbb{N}_3, \ldots, \mathbb{N}_9$ are the constants in general solution.

3.1 Convergence of HAM

The $\hbar-$ curve, also identified as factor for convergence controlling, was familiarized by Liao [51–53]. In Figure 2,

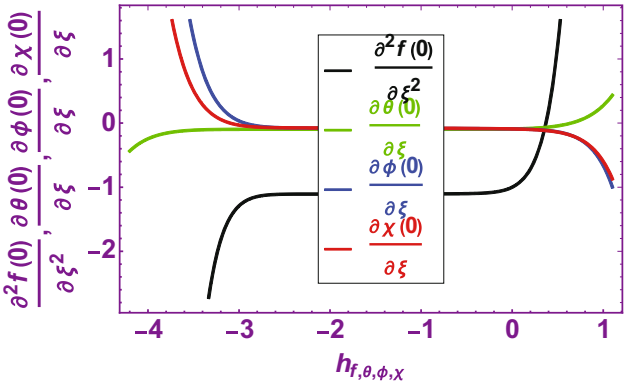

Figure 2: $\hbar$ curves for $\frac{\partial^2 f(0)}{\partial \xi^2}$, $\frac{\partial \theta(0)}{\partial \xi}$, $\frac{\partial \phi(0)}{\partial \xi}$, and $\frac{\partial \chi(0)}{\partial \xi}$.

we have fixed the convergence regions of $\frac{\partial^2 f(0)}{\partial \xi^2}$, $\frac{\partial \theta(0)}{\partial \xi}$, $\frac{\partial \phi(0)}{\partial \xi}$, and $\frac{\partial \chi(0)}{\partial \xi}$. The respective convergence regions of $\frac{\partial^2 f(0)}{\partial \xi^2}$, $\frac{\partial \theta(0)}{\partial \xi}$, $\frac{\partial \phi(0)}{\partial \xi}$, and $\frac{\partial \chi(0)}{\partial \xi}$ are $-3.0 \le \hbar_f \le 0.0$, $-3.5 \le \hbar_\theta \le 0.5$, $-3.0 \le \hbar_\phi \le 0.2$, and $-3.0 \le \hbar_\chi \le 0.2$. Additionally, the squared residual error along with CPU time for $\frac{\partial^2 f(\xi)}{\partial \xi^2}$, $\frac{\partial \theta(\xi)}{\partial \xi}$, $\frac{\partial \phi(\xi)}{\partial \xi}$, and $\frac{\partial \chi(\xi)}{\partial \xi}$ are displayed in Table 2. Furthermore, the HAM is compared with numerical technique and a great agreement has been found between both techniques as shown in Tables 2–5.

4 Results and discussion

The physical interpretation of the Walters-B nanoliquid past a linearly extending sheet with slip and convective conditions has been presented and discussed in detail in Figures 3–23 and Tables 3–7. The slip condition is imposed on velocity field to investigate the nanofluid motion. The Walters-B nanofluid contains the gyrotactic microorganisms and nanoparticles. The mixed convective phenomenon along with magnetic field impact is taken into consideration.

Table 2: Squared residual errors at dissimilar direction of estimations

Approximation order	CPU time (s)	Velocity profile	Temperature profile	Concentration profile	Density profile
1	0.140631	2.73417×10^{-7}	0.000010	2.17824×10^{-6}	0.000214
5	0.921921	2.0221×10^{-9}	4.14596×10^{-6}	7.64851×10^{-8}	0.000081
7	2.875159	2.7662×10^{-11}	2.80687×10^{-6}	3.0774×10^{-9}	0.000034
9	7.32851	2.29879×10^{-13}	1.85264×10^{-6}	1.47975×10^{-10}	0.000014
11	17.1884	3.48909×10^{-15}	1.53309×10^{-6}	8.69921×10^{-12}	7.33828×10^{-6}
13	44.096	1.84024×10^{-17}	1.13897×10^{-6}	6.21891×10^{-13}	4.21847×10^{-6}
15	117.553	7.3059×10^{-20}	9.681×10^{-7}	5.10918×10^{-14}	2.85843×10^{-6}

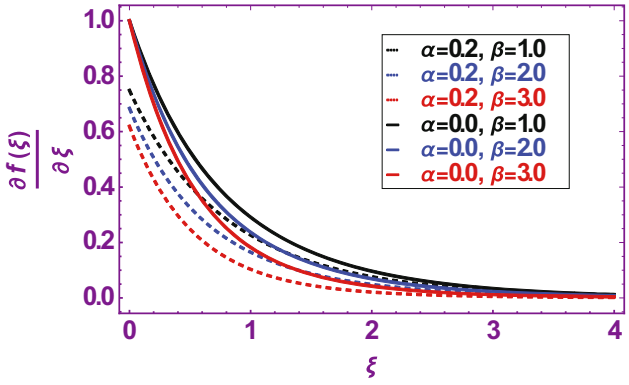

Figure 3: Impact of β on $\frac{\partial f(\xi)}{\partial \xi}$.

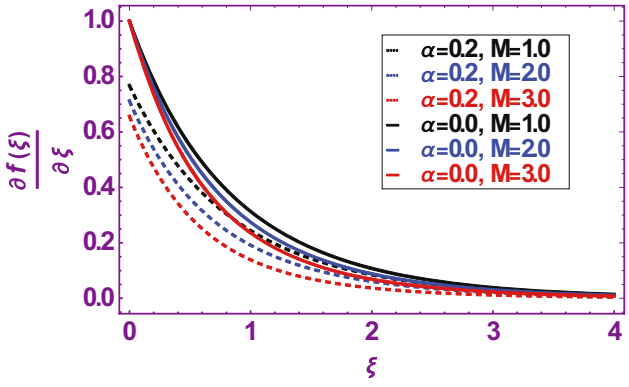

Figure 4: Impact of M on $\frac{\partial f(\xi)}{\partial \xi}$.

4.1 Velocity profiles

Figures 3 and 4 show the variation in $\frac{\partial f(\xi)}{\xi}$ *via* β and M, respectively, for the both α = 0.2 and α = 0.0. The enhancing β and M have reduced $\frac{\partial f(\xi)}{\xi}$. When β increases, the velocity boundary layer becomes weak. As β increases, tensile stresses increase which impedes momentum transport as indicated in Figure 3. The greater M reduces $\frac{\partial f(\xi)}{\xi}$. This effect is due to the Lorentz force, which always retarded the fluid motion. Thus, decreasing impact is found here. On the other hand, considering velocity-offset and no-velocity-offset conditions, impressions of β and M are dominant for the case of velocity-offset condition. Additionally, the impacts of these parameters are dominant

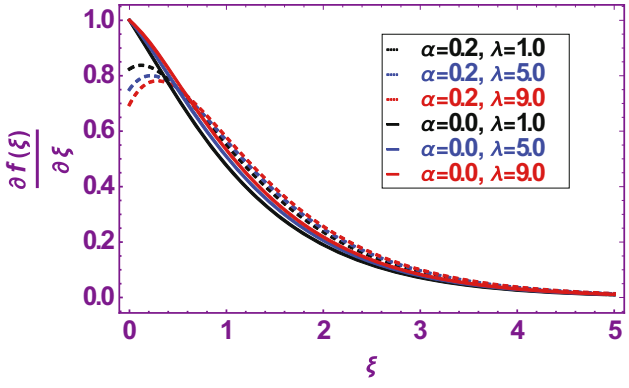

Figure 5: Impact of λ on $\frac{\partial f(\xi)}{\partial \xi}$.

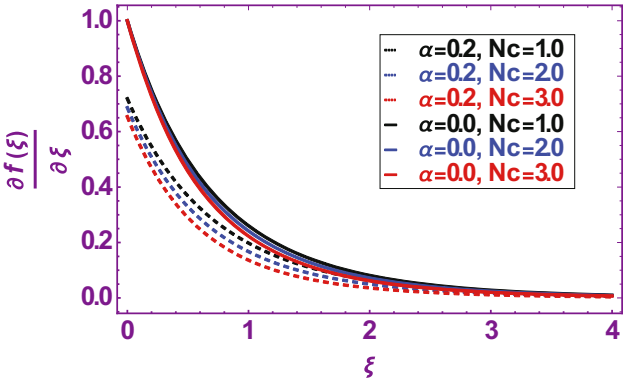

Figure 6: Impact of Nc on $\frac{\partial f(\xi)}{\partial \xi}$.

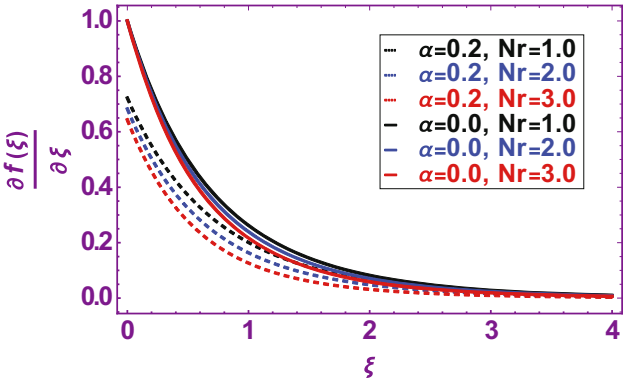

Figure 7: Impact of Nr on $\frac{\partial f(\xi)}{\partial \xi}$.

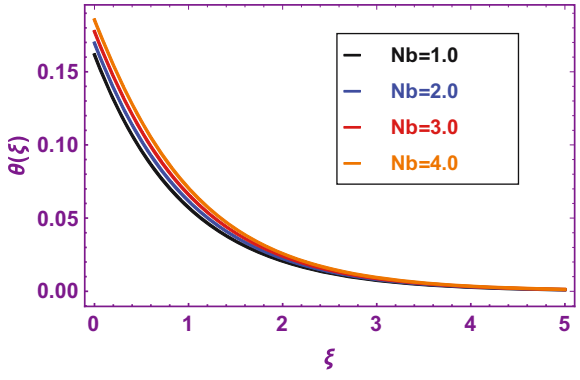

Figure 8: Impact of Nb on $\theta(\xi)$.

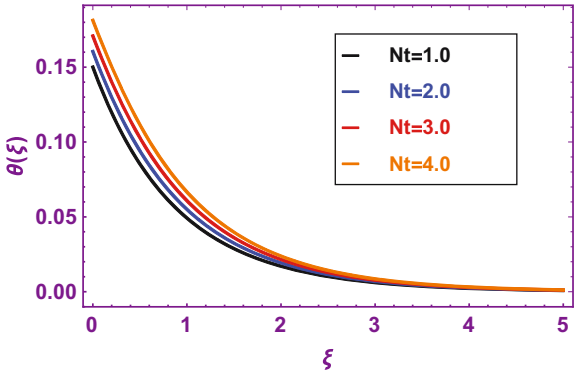

Figure 9: Impact of Nt on $\theta(\xi)$.

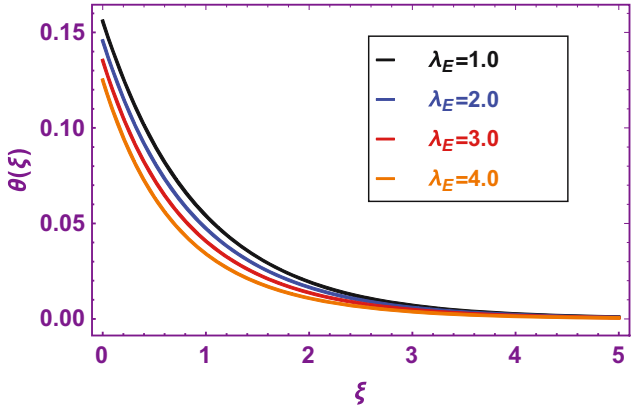

Figure 10: Impact of λ_E on $\theta(\xi)$.

for $\alpha = 0.2$. Figure 5 indicates the impact of λ on $\frac{\partial f(\xi)}{\xi}$ for both $\alpha = 0.2$ and $\alpha = 0.0$. The augmenting λ augments the nanofluid motion for both $\alpha = 0.2$ and $\alpha = 0.0$. The increasing λ strengthens the buoyancy force which results in the augmenting conduct in nanofluid motion. Thus, the boosting impact is observed here. Additionally, the slip

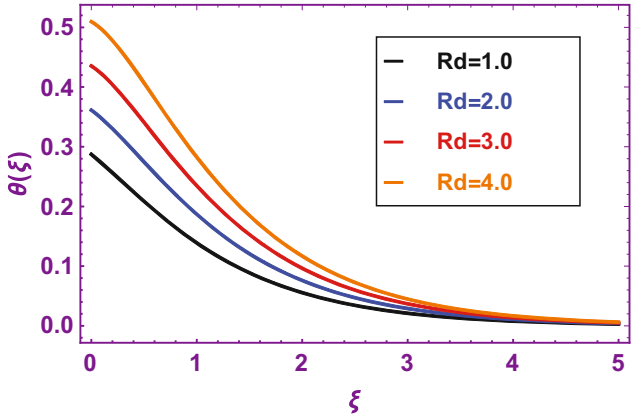

Figure 11: Impact of Rd on $\theta(\xi)$.

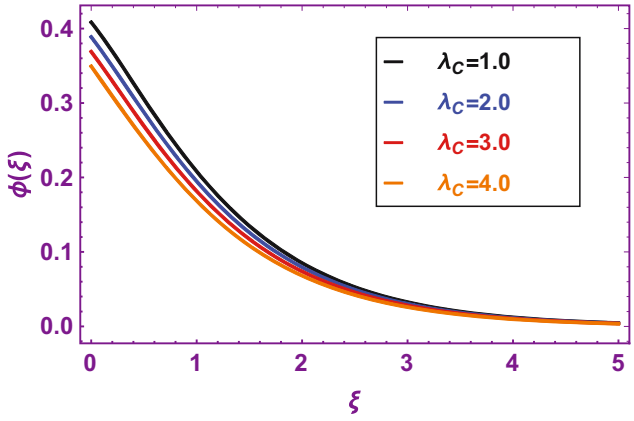

Figure 12: Impact of λ_C on $\phi(\xi)$.

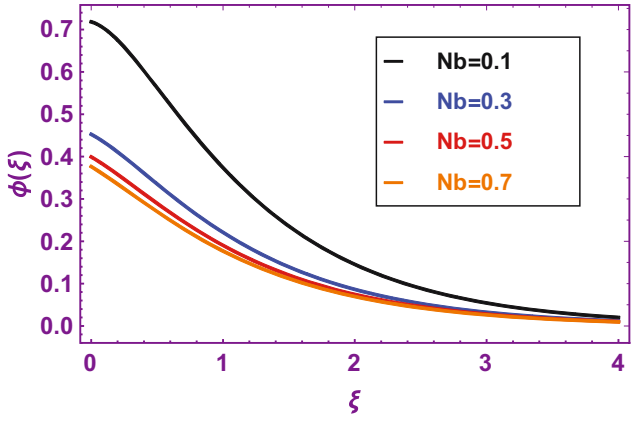

Figure 13: Impact of Nb on $\phi(\xi)$.

condition reduces the fluid motion, say $0 < \xi < 0.5$. However, away from the stretching surface say $0.5 < \xi < \infty$, an increasing conduct up to some points and then free stream velocity is found. Figure 6 indicates the impact of Nc on $\frac{\partial f(\xi)}{\xi}$ for both $\alpha = 0.2$ and $\alpha = 0.0$. The augmenting

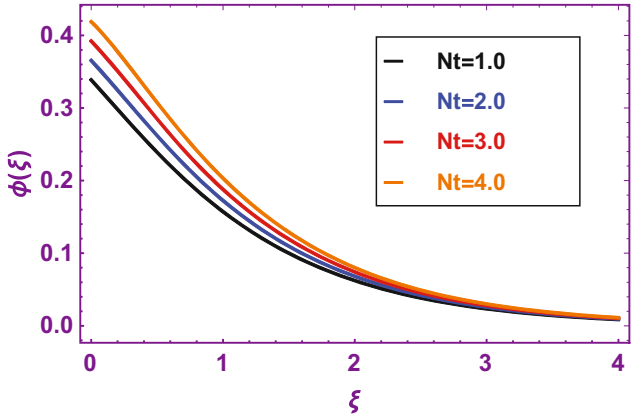

Figure 14: Impact of Nt on $\phi(\xi)$.

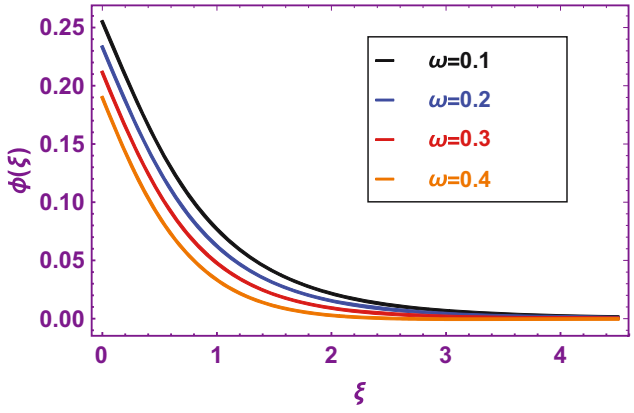

Figure 15: Impact of ω on $\phi(\xi)$.

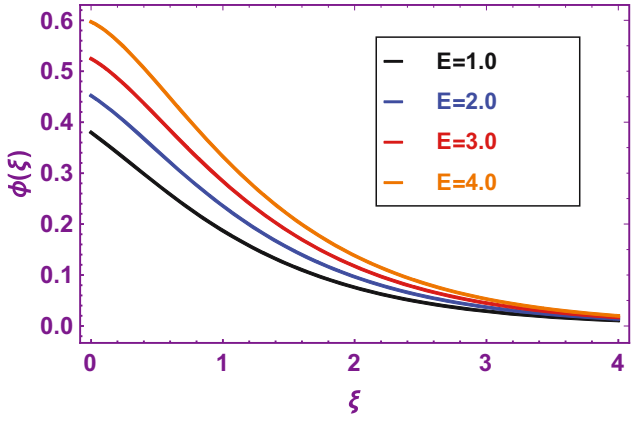

Figure 16: Impact of E on $\phi(\xi)$.

Nc decreases the nanofluid motion for both $\alpha = 0.2$ and $\alpha = 0.0$. The reducing impact of Nc on $\frac{\partial f(\xi)}{\xi}$ is dominant for $\alpha = 0.2$ as compared to $\alpha = 0.0$. Figure 7 indicates the impact of Nr on $\frac{\partial f(\xi)}{\xi}$ for both $\alpha = 0.2$ and $\alpha = 0.0$. The escalating Nr reduces $\frac{\partial f(\xi)}{\xi}$ for both $\alpha = 0.2$ and $\alpha = 0.0$. The

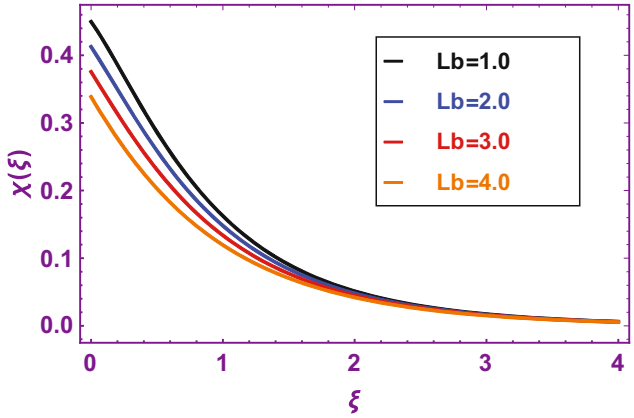

Figure 17: Impact of Lb on $\chi(\xi)$.

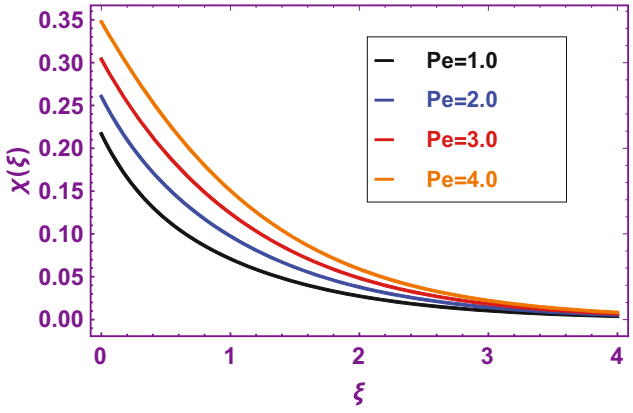

Figure 18: Impact of Pe on $\chi(\xi)$.

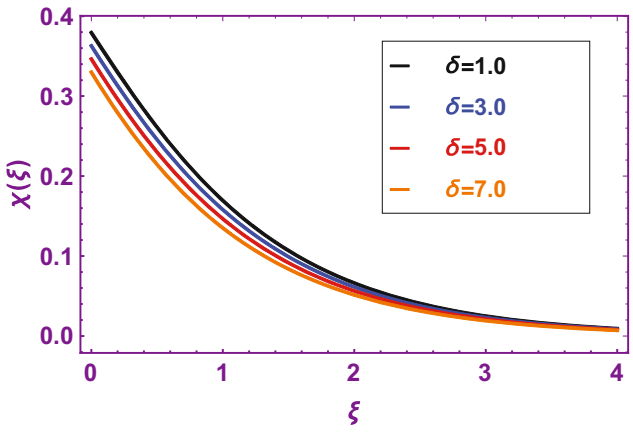

Figure 19: Impact of δ on $\chi(\xi)$.

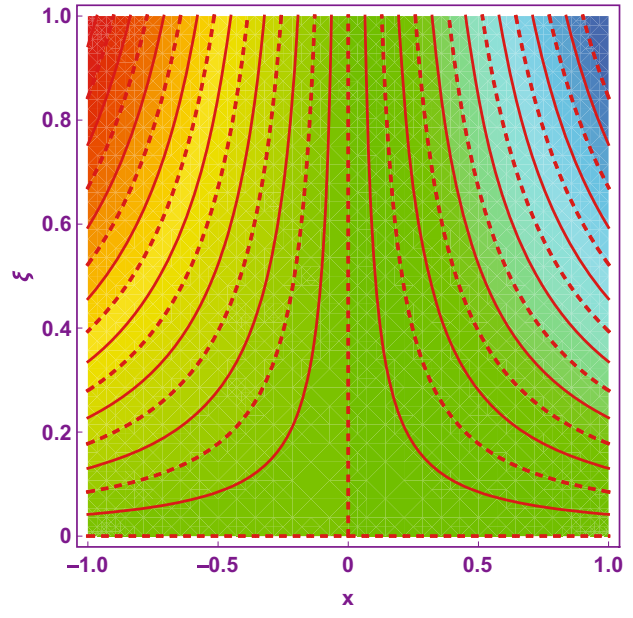

Figure 20: Streamline patterns for Newtonian case.

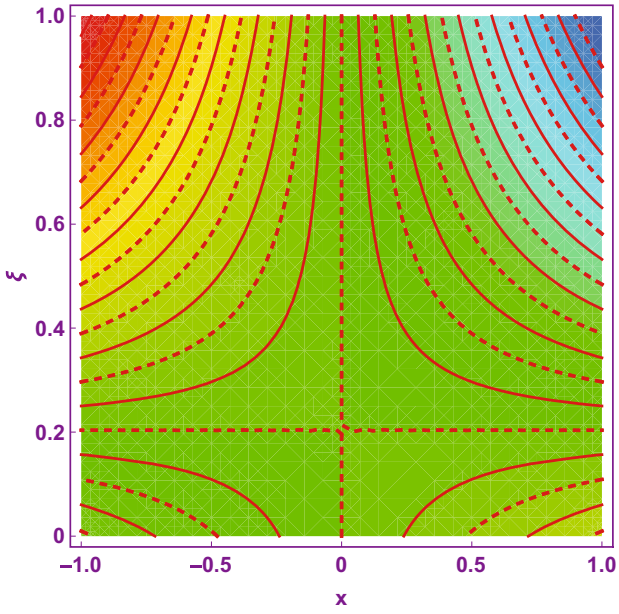

Figure 21: Streamline patterns for non-Newtonian case.

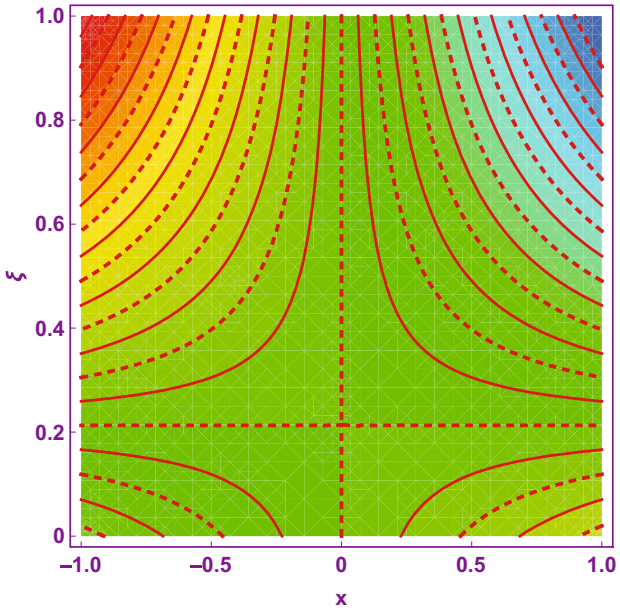

Figure 23: Streamline patterns for magnetized case.

reducing impact of Nr on $\frac{\partial f(\xi)}{\xi}$ is dominant for $\alpha = 0.2$ as compared to $\alpha = 0.0$.

4.2 Temperature profiles

Figure 8 signifies the impact of Nb on $\theta(\xi)$. The increase in Nb augments $\theta(\xi)$. The random motion of particles is known as Brownian motion. As Nb increases, the particles start colliding due to random motion, which eventually increases the fluid temperature. Thus, the increasing impact of Nb on $\theta(\xi)$ is reported. Figure 9 signifies the impact of Nt on $\theta(\xi)$. The increase in Nt augments $\theta(\xi)$. Physically, the increase in Nt moves the nanofluid nanoparticles from warm region to cold region, which consequently augments the temperature layer thickness and thermal profile. Figure 10 indicates the impact of λ_E on $\theta(\xi)$. The λ_E parameter reduces $\theta(\xi)$. When λ_E is increased, the temperature drops and the profile smoothly descends to zero at a closer distance from the sheet. When the relaxation period for heat flux is longer, the thermal boundary layer will be thinner. As temperature relaxation parameter increases, the profile

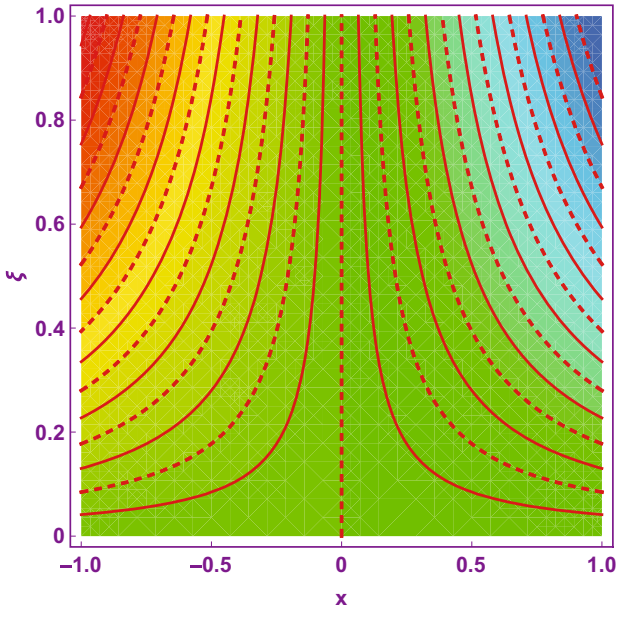

Figure 22: Streamline patterns for non-magnetized case.

Table 3: Comparison of the present results of $-\frac{\partial^2 f(0)}{\partial \xi^2}$ with previously published results, when $\lambda = 0.0$, Nr = 0.0, Nc = 0.0, and $\alpha = 0.0$

β	Pillai *et al.* [54]	Mahantesh *et al.* [14]	Present results
0.0	1.00000	1.00000	1.05040
0.0001	1.00005	1.00005	1.05046
0.001	1.00050	1.00050	0.05059
0.005	—	1.00251	1.05121
0.01	1.00504	1.00504	1.05200
0.03	—	1.01535	1.05533
0.05	—	1.02598	1.05896
0.1	1.05409	1.05409	1.05954
0.2	1.11803	1.11803	1.10654
0.3	1.19523	1.19523	1.17411
0.4	1.29099	1.29099	1.27307
0.5	1.41421	1.41421	1.40194

Table 4: Numerical outcomes of the skin friction *vs* embedded parameters

β	M	λ	Nr	Nc	$2(1-3\beta)\frac{\partial^2 f(0)}{\partial \xi^2}$	
					$\alpha = 0.2$	$\alpha = 0.0$
0.1	0.1	0.1	0.1	0.1	−0.583876	−0.726352
0.2					−0.336899	−0.422872
0.3					−0.085038	−0.107671
0.1	0.2				−0.590713	−0.740026
	0.3				−0.597549	−0.753699
	0.4				−0.604346	−0.767372
	0.1	0.2			−0.583279	−0.725358
		0.3			−0.582683	−0.724363
		0.4			−0.582086	−0.723369
		0.1	0.2		−0.583981	−0.726477
			0.3		−0.584025	−0.726601
			0.4		−0.584100	−0.726725
			0.1	0.2	−0.583981	−0.726477
				0.3	−0.584025	−0.726601
				0.4	−0.584100	−0.726725

progresses steeper in the neighborhood of the boundary, indicating that the temperature wall slope is increasing. Figure 11 shows the impact of Rd on $\theta(\xi)$. The higher Rd augments $\theta(\xi)$. Physically, when we apply Rd effect, the surface heat flux increases; consequently, the heat flux becomes the key point to increase the temperature curve. Thus, an increasing conduct is found here.

4.3 Concentration profiles

Figure 12 indicates the impact of λ_C on $\phi(\xi)$. The higher λ_C reduces $\phi(\xi)$. When λ_C is increased, the concentration drops and the profile smoothly descends to zero at a closer distance from the sheet. When the relaxation period for mass flux is longer, the concentration boundary layer will be thinner. As λ_C, the profile progressively steeper in the neighborhood of the boundary, indicating that the concentration wall slope is increasing. Figure 13 signifies the impact of Nb on $\phi(\xi)$. The escalating Nb reduces $\phi(\xi)$. When nanoparticles are incorporated into a fluid, Brownian diffusion and thermophoresis parameters develop. Brownian diffusion and thermophoresis characteristics are useful in determining how nanoparticles move in a fluid. It has been established that greater Brownian motion values are the fundamental reason for the increase in random motion. The fluid's mass decreases as a result of this. On the other hand, the escalating Nt augments $\phi(\xi)$ as shown in

Table 5: Numerical outcomes of the Nusselt number

Rd	Nb	Nt	λ_E	Pr	$-(1+\text{Rd})\frac{\partial \theta(0)}{\partial \xi}$
0.1	0.1	0.1	0.1	1.0	0.099975
0.2					0.108871
0.3					0.117733
0.1	0.2				0.099963
	0.3				0.099951
	0.4				0.099939
	0.1	0.2			0.099963
		0.3			0.099951
		0.4			0.099939
		0.1	0.2		0.100153
			0.3		0.100331
			0.4		0.100509
			0.1	1.5	0.100627
				3.4	0.101355
				6.0	0.101604

Table 6: Numerical outcomes of the Sherwood number

Le	Nb	Nt	λ_C	E	ω	$\frac{\partial \phi(0)}{\partial \xi}$
0.1	0.1	0.1	0.1		0.1	0.089739
0.2						0.090294
0.3						0.090849
0.1	0.2					0.090904
	0.3					0.090922
	0.4					0.090931
	0.1	0.2				0.090739
		0.3				0.090629
		0.4				0.090519
		0.1	0.2			0.091139
			0.3			0.091430
			0.4			0.092178
			0.1	0.2		0.089906
				0.3		0.089880
				0.4		0.089854
				0.1	0.2	0.089906
					0.3	0.089890
					0.4	0.089854

Table 7: Numerical values of the density number *via* different embedded parameters

Lb	Pe	δ	$-\frac{\partial \chi(0)}{\partial \xi}$
0.1	0.1	0.1	0.089252
0.2			0.089171
0.3			0.089090
0.1	0.2		0.089290
	0.3		0.089328
	0.4		0.089366
	0.1	0.2	0.089268
		0.3	0.089284
		0.4	0.089300

Figure 14. Figure 15 represents the impact of ω on $\phi(\xi)$. The increasing ω decreases $\phi(\xi)$. The mass boundary layer thickens with the increase in ω. The increasing ω enhances the term $\omega(\sigma\theta + 1)^n \exp[-E/(\sigma\theta + 1)]$, which consequently augments the concentration of the nanofluid flow. Thus, an increasing impact is found here. Figure 16 shows the impact of E on $\phi(\xi)$. The increasing E augments $\phi(\xi)$. The activation energy is defined as the least energy required to initiate a reaction. It is discovered that at low temperatures and higher activation energies, the reaction rate constant decreases, resulting in a slowing of the chemical process as well as an increase in $\phi(\xi)$.

4.4 Density profiles

The impacts of Lb and Pe on $\chi(\xi)$ are displayed in Figures 17 and 18. The increasing Lb and Pe reduce $\chi(\xi)$. As the Lewis number rises, the microorganisms' diffusivity falls while the viscous diffusion rate rises, the motile density boundary layer thickness is reduced as a result. A rise in Pe improves the motile density boundary layer thickness and augments $\chi(\xi)$. This is due to an inverse relation of Pe microorganisms' diffusivity with a constant chemotaxis constant. This means that as the parameter is increased, the floating speed dominates the diffusivity of the microorganisms, resulting in a rise in motile microorganism density. Figure 19 displays the impact of δ on $\chi(\xi)$. The augmenting δ reduces $\chi(\xi)$.

4.5 Streamline patterns

Figures 20 and 21 show the streamline patterns of two different Newtonian and NNF cases, respectively. It is clear from the figures that the streamline patterns are quite different for the Newtonian and non-Newtonian cases. Figures 22 and 23 show the streamline patterns for magnetized and non-magnetized cases, respectively. It is clear from the figures that the streamline patterns are quite different for both cases. This behavior is due to the fact that the higher magnetic field produces friction force at the surface of sheet which results in the reduction in the flow velocity as discussed in Figure 4. As a result, the streamlines become closer when compared to the non-magnetized fluid flow.

4.6 Quantities of interest

This section deals with the influences of physical parameters on skin friction, heat transfer, mass transfer, and density number. Table 3 guarantees the validation of the present model with previously published results. Table 4 shows the impacts of β, M, λ, Nr, and Nc on skin friction for both slip and no-slip conditions. The augmenting β and λaugment the skin friction, whereas the increase in$M$, Nr, and Nc reduces the skin friction. Table 5 shows the impacts of Rd, Nb, Nt, λ_E, and Pr on Nusselt number. The augmenting Rd, λ_E, and Pr augment the Nusselt number, whereas the increase in Nb and Nt reduces the Nusselt number. Table 6 shows the impacts of Le, Nb, Nt, λ_C, E, and ω on Sherwood number. The augmenting Le, Nb, and λ_C augment the Sherwood number, whereas the increase in Nt, E, and ω reduces the Sherwood number. Table 7 shows the impacts of Lb, Pe, and δ on the density number. The augmenting Pe and δ augment the density number, whereas the increase in Lb reduces the density number.

5 Conclusion

In this analysis we have studied the mixed convection flow of Walters-B fluid past an extending surface. The Walters-B nanofluid contains the gyrotactic microorganisms and nanoparticles. The convective and slip conditions are taken into consideration. The physical interpretation of the embedded parameters on Walters-B nanofluid has been presented and discussed. The slip condition is imposed on velocity field to investigate the nanofluid motion. Also, the convective conditions are taken in temperature, nanoparticles concentration, and microorganisms concentration equations. The concluding remarks are listed as:

1) The escalated viscoelastic, magnetic, and buoyancy ratio factor have declined the nanofluid motion for both slip and no-slip conditions. These impacts are dominant for the case of slip condition.
2) The augmented mixed convection parameter has increased the nanofluid motion for both slip and no-slip conditions. Additionally, at the surface of sheet, the slip condition reduces the fluid motion, say $0 < \xi < 0.5$. However, away from the stretching surface say $0.5 < \xi < \infty$, an increasing conduct up to some points and then free stream velocity is found.
3) The escalated Brownian motion, thermophoresis, and thermal radiation parameters have escalated the thermal profile, while the augmented temperature relaxation parameter has reduced the temperature profile.
4) The escalated thermophoresis and activation energy have augmented the concentration profile, whereas the escalated concentration relaxation, Brownian motion, and chemical reaction parameters have reduced the concentration profile.

5) The increased bioconvection Lewis number has increased the microorganisms' profile while the greater bioconvection Peclet number has increased the microorganisms' profiles reduced.
6) The increased Lewis number and Peclet number decrease the density function.
7) The streamline patterns for Newtonian, non-Newtonian, magnetized, and non-magnetized cases have different behaviors.

Funding information: This work was supported by the Deanship of Scientific Research, the Vice Presidency for Graduate Studies and Scientific Research, King Faisal University, Saudi Arabia (Grant No. 4711).

Author contributions: All authors have accepted responsibility for the entire content of this manuscript and approved its submission.

Conflict of interest: The authors have no conflict of interest.

Data availability statement: All data generated or analyzed during this study are included in this published article.

References

[1] Turkyilmazoglu M. Three dimensional MHD flow and heat transfer over a stretching/shrinking surface in a viscoelastic fluid with various physical effects. Int J Heat Mass Transf. 2014;78:150–5. doi: 10.1016/J.IJHEATMASSTRANSFER.2014.06.052.
[2] Hosseini M, Sheikholeslami Z, Ganji DD. Non-Newtonian fluid flow in an axisymmetric channel with porous wall. Propuls Power Res. 2013;2:254–62. doi: 10.1016/J.JPPR.2013.10.001.
[3] Abbasbandy S, Naz R, Hayat T, Alsaedi A. Numerical and analytical solutions for Falkner–Skan flow of MHD Maxwell fluid. Appl Math Comput. 2014;242:569–75. doi: 10.1016/J.AMC.2014.04.102.
[4] Yang D, Zhu KQ. Start-up flow of a viscoelastic fluid in a pipe with a fractional Maxwell's model. Comput Math Appl. 2010;60:2231–8. doi: 10.1016/J.CAMWA.2010.08.013.
[5] Hayat T, Safdar A, Awais M, Mesloub S. Soret and Dufour effects for three-dimensional flow in a viscoelastic fluid over a stretching surface. Int J Heat Mass Transf. 2012;55:2129–36. doi: 10.1016/J.IJHEATMASSTRANSFER.2011.12.016.
[6] Hayat T, Shehzad SA, Qasim M. Mixed convection flow of a micropolar fluid with radiation and chemical reaction. Int J Numer Methods Fluids. 2011;67:1418–36. doi: 10.1002/FLD.2424.
[7] Jamil M, Rauf A, Fetecau C, Khan NA. Helical flows of second grade fluid due to constantly accelerated shear stresses. Commun Nonlinear Sci Numer Simul. 2011;16:1959–69. doi: 10.1016/J.CNSNS.2010.09.003.
[8] Mustafa M, Hayat T, Pop I, Hendi A. Stagnation-point flow and heat transfer of a Casson fluid towards a stretching sheet. Z Naturforsch - Sect A J Phys Sci. 2012;67:70–6. doi: 10.5560/ZNA.2011-0057/MACHINEREADABLECITATION/RIS.
[9] Mushtaq A, Mustafa M, Hayat T, Alsaedi A. Effects of thermal radiation on the stagnation-point flow of upper-convected maxwell fluid over a stretching sheet. J Aerosp Eng. 2013;27:04014015. doi: 10.1061/(ASCE)AS.1943-5525.0000361.
[10] Hayat T, Shafiq A, Alsaedi A. Effect of Joule heating and thermal radiation in flow of third grade fluid over radiative surface. PLoS One. 2014;9:e83153. doi: 10.1371/JOURNAL.PONE.0083153.
[11] Bhatia PK, Steiner JM. Convective instability in a rotating viscoelastic fluid layer. ZAMM - J Appl Math Mech/Z Angew Math Mech. 1972;52:321–7. doi: 10.1002/ZAMM.19720520601.
[12] Beard DW, Walters K. Elastico-viscous boundary-layer flows I. Two-dimensional flow near a stagnation point. Math Proc Cambridge Philos Soc. 1964;60:667–74. doi: 10.1017/S0305004100038147.
[13] Sharma V, Gupta U. Stability of stratified elasto-viscous Walter's (Model B') fluid in the presence of horizontal magnetic field and rotation. Stud Geotech Mech. 2010;32:41–53.
[14] Nandeppanavar MM, Abel MS, Tawade J. Heat transfer in a Walter's liquid B fluid over an impermeable stretching sheet with non-uniform heat source/sink and elastic deformation. Commun Nonlinear Sci Numer Simul. 2010;15:1791–802. doi: 10.1016/J.CNSNS.2009.07.009.
[15] Abdul Hakeem AK, Vishnu Ganesh N, Ganga B. Effect of heat radiation in a Walter's liquid B fluid over a stretching sheet with non-uniform heat source/sink and elastic deformation. J King Saud Univ - Eng Sci. 2014;26:168–75. doi: 10.1016/J.JKSUES.2013.05.006.
[16] Makinde OD, Gnaneswara Reddy M, Venugopal Reddy K. Effects of thermal radiation on MHD peristaltic motion of walters-B fluid with heat source and slip conditions. J Appl Fluid Mech. 2017;10:1105–12. doi: 10.18869/ACADPUB.JAFM.73.241.27082.
[17] Tahir M, Naeem MN, Javaid M, Younas M, Imran M, Sadiq N, et al. Unsteady flow of fractional Oldroyd-B fluids through rotating annulus. Open Phys. 2018;16:193–200.
[18] Waqas H, Imran M, Muhammad T, Sait SM, Ellahi R. On bio-convection thermal radiation in Darcy–Forchheimer flow of nanofluid with gyrotactic motile microorganism under Wu's slip over stretching cylinder/plate. Int J Numer Methods Heat Fluid Flow. 2021;31:1520–46.
[19] Imran M, Farooq U, Waqas H, Anqi AE, Safaei MR. Numerical performance of thermal conductivity in bioconvection flow of cross nanofluid containing swimming microorganisms over a cylinder with melting phenomenon. Case Stud Therm Eng. 2021;26:101181.
[20] Ibrahim SM, Kumar PV, Lorenzini G. Influence of thermophoresis and Brownian motion of nanoparticles on radiative chemically-reacting MHD Hiemenz flow over a nonlinear stretching sheet with heat generation. Fluid Dyn Mater Process. 2023;19(4):855–68.
[21] Kumar PV, Sunitha C, Ibrahim SM, Lorenzini G. Outlining the slip effects on MHD Casson nanofluid flow over a permeable stretching sheet in the existence of variable wall thickness. J Eng Thermophys. 2023;32:69–88.
[22] Sekhar PR, Sreedhar S, Ibrahim SM, Kumar PV. Radiative heat source fluid flow of MHD Casson nanofluid over a non-linear inclined surface with Soret and Dufour effects. CFD Lett. 2023;15:42–60.
[23] Harish M, Ibrahim SM, Kumar PV, Lorenzini G. A study on effects of thermal radiative dissipative MHD non-Newtonian nanofluid above an elongating sheet in porous medium. J Appl Comput Mech. 2023;9(4):945–54.

[24] Swain K, Animasaun IL, Ibrahim SM. Influence of exponential space-based heat source and Joule heating on nanofluid flow over an elongating/shrinking sheet with an inclined magnetic field. Int J Ambient Energy. 2022;43:4045–57. doi: 10.1080/01430750.2021.1873854.
[25] Singh JK, Vishwanath S. Hall and induced magnetic field effects on MHD buoyancy-driven flow of Walter's-B fluid over a magnetised convectively heated inclined surface. Int J Ambient Energy. 2023;43(1). doi: 10.1080/01430750.2021.1909652.
[26] Qaiser D, Zheng Z, Riaz Khan M. Numerical assessment of mixed convection flow of Walter's-B nanofluid over a stretching surface with Newtonian heating and mass transfer. Therm Sci Eng Prog. 2021;22:100801. doi: 10.1016/J.TSEP.2020.100801.
[27] Akinbo BJ, Olajuwon BI. Impact of radiation and chemical reaction on stagnation-point flow of Hydromagnetic Walter's-B fluid with Newtonian heating. Int Commun Heat Mass Transf. 2021;121:105115. doi: 10.1016/J.ICHEATMASSTRANSFER.2021.105115.
[28] Sunthrayuth P, Alderremy A, Aly S, Shah R, Akgül A. Exact analysis of electro-osmotic flow of Walter's-B fluid with non-singular kernel. Pramana. 2021;95:1–10. doi: 10.1007/S12043-021-02224-8.
[29] Akinbo BJ, Olajuwon BI. Radiation and thermal-diffusion interaction on stagnation-point flow of Walter's-B fluid toward a vertical stretching sheet. Int Commun Heat Mass Transf. 2021;126:105471. doi: 10.1016/J.ICHEATMASSTRANSFER.2021.105471.
[30] Ahmad I, Faisal M, Javed T. Unsteady flow of walter's-B magneto-nanofluid over a bidirectional stretching surface in a porous medium with heat generation. Spec Top Rev Porous Media An Int J. 2021;12:49–70. doi: 10.1615/SPECIALTOPICSREVPOROUSMEDIA.2020034320.
[31] Akinbo BJ, Olajuwon BI. Heat transfer analysis in a hydromagnetic Walter's-B fluid with elastic deformation and Newtonian heating. Heat Transf. 2021;50:2033–48. doi: 10.1002/HTJ.21967.
[32] He J-H, Moatimid GM, Sayed A. Nonlinear EHD instability of two-superposed walter's-B fluids moving through porous media. Axioms. 2021;10:258. doi: 10.3390/AXIOMS10040258.
[33] Siddique I, Shah NA, Abro KA. Thermography of ferromagnetic Walter's-B fluid through varying thermal stratification. S Afr J Chem Eng. 2021;36:118–26. doi: 10.1016/J.SAJCE.2020.12.004.
[34] Qayyum S, Hayat T, Jabeen S, Alsaedi A. Entropy generation in nanofluid flow of Walter's-B fluid with homogeneous-heterogeneous reactions. Math Methods Appl Sci. 2020;43:5657–72. doi: 10.1002/MMA.5997.
[35] Farooq U, Tahir M, Waqas H, Muhammad T, Alshehri A, Imran M. Investigation of 3D flow of magnetized hybrid nanofluid with heat source/sink over a stretching sheet. Sci Rep. 2022;12:1–15. doi: 10.1038/s41598-022-15658-w.
[36] Farooq U, Imran M, Fatima N, Noreen S, Tahir M, Akgül A, et al. Cattaneo-Christov heat flux model in radiative flow of (Fe_3O_4–TiO_2/Transformer oil) and (Cu–TiO_2/Transformer oil) magnetized hybrid nanofluids past through double rotating disks. Case Stud Therm Eng. 2023;45:102905.
[37] Wakif A, Animasaun IL, Narayana PVS, Sarojamma G. Meta-analysis on thermo-migration of tiny/nano-sized particles in the motion of various fluids. Chin J Phys. 2020;68:293–307.
[38] Manigandan A, Satya Narayana PV. Influence of variable thermal conductivity and mixed convection on hybrid nanofluid (SWCNT + MWCNT/H_2O) flow over an exponentially elongated sheet with slip conditions. Indian J Phys. 2023;1–14.
[39] Madiha Takreem K, Satya Narayana PV. Impacts of Joule heating and dissipation on magnetohydrodynamic ternary-hybrid nanofluid (Al_2O_3-TiO_2-SiO_2/H_2O) flow over an elongated sheet with Darcy–Forchheimer medium. Proc Inst Mech Eng Part E J Process Mech Eng. 2023;09544089231200381.
[40] Harish Babu D, Naidu KK, Deo S, Satya Narayana PV. Impacts of inclined Lorentz forces on hybrid CNTs over an exponentially stretching sheet with slip flow. Int J Model Simul. 2023;43:310–24.
[41] Harish Babu D, Venkateswarlu B, Sarojamma G, Satya Narayana PV. Coupled impression of radiative thermal flux and Lorentz force on the water carrying composite nanoliquid streaming past an elastic sheet. J Therm Sci Eng Appl. 2022;14:91002.
[42] Venkateswarlu B, Satya Narayana PV. Coriolis force impact on the magnetorotating fluid radiating from a moving porous upright plate with viscous dissipation. Heat Transf. 2023;52:4227–52.
[43] Zhang K, Shah NA, Alshehri M, Alkarni S, Wakif A, Eldin SM. Water thermal enhancement in a porous medium via a suspension of hybrid nanoparticles: MHD mixed convective Falkner's-Skan flow case study. Case Stud Therm Eng. 2023;47:103062.
[44] Wakif A, Shah NA. Hydrothermal and mass impacts of azimuthal and transverse components of Lorentz forces on reacting Von Kármán nanofluid flows considering zero mass flux and convective heating conditions. Waves Random Complex Media. 2022;1–22.
[45] Ragupathi P, Ahammad NA, Wakif A, Shah NA, Jeon Y. Exploration of multiple transfer phenomena within viscous fluid flows over a curved stretching sheet in the co-existence of gyrotactic microorganisms and tiny particles. Mathematics. 2022;10:4133.
[46] Rasool G, Wakif A, Wang X, Alshehri A, Saeed AM. Falkner-Skan aspects of a radiating (50% ethylene glycol + 50% water)-based hybrid nanofluid when Joule heating as well as Darcy-Forchheimer and Lorentz forces affect significantly. Propuls Power Res. 2023;12(3):428–42.
[47] Areekara S, Sabu AS, Mathew A, Parvathy KS, Wakif A. Significance of nanoparticle radius on EMHD Casson nanomaterial flow with non-uniform heat source and second-order velocity slip. Numer Heat Transf Part B Fundam. 2023;1–18.
[48] Babu KSS, Parandhama A, Vijaya RB. Non-linear MHD convective flow of Carreau nanofluid over an exponentially stretching surface with activation energy and viscous dissipation. SN Appl Sci. 2021;3:382.
[49] Daniel YS, Aziz ZA, Ismail Z, Salah F. Effects of slip and convective conditions on MHD flow of nanofluid over a porous nonlinear stretching/shrinking sheet. Aust J Mech Eng. 2018;16:213–29.
[50] Liao S-J. The proposed homotopy analysis technique for the solution of nonlinear problems. Doctoral dissertation, Shanghai Jiao Tong University; 1992.
[51] Liao S. An optimal homotopy-analysis approach for strongly nonlinear differential equations. Commun Nonlinear Sci Numer Simul. 2010;15:2003–16. doi: 10.1016/J.CNSNS.2009.09.002.
[52] Liao S. Beyond perturbation: introduction to the homotopy analysis method; 2004. p. 322.
[53] Liao S. Introduction. Homotopy Analysis Method in Nonlinear Differential Equations. Heidelberg: Springer Berlin; 2012. p. 3–14. doi: 10.1007/978-3-642-25132-0_1.
[54] Pillai KMC, Sai KS, Swamy NS, Nataraja HR, Tiwari SB, Rao BN. Heat transfer in a viscoelastic boundary layer flow through a porous medium. Comput Mech. 2004;34:27–37. doi: 10.1007/S00466-004-0550-8.